

# CORTISTATIN REGULATES FIBROSIS AND MYOFIBROBLAST ACTIVATION IN EXPERIMENTAL HEPATOTOXIC- AND CHOLESTATIC-INDUCED LIVER INJURY

Raquel Benitez<sup>1</sup>, Marta Caro<sup>1</sup>, Eduardo Andrés-León<sup>2</sup>, Francisco O’Valle<sup>3</sup>, and Mario Delgado<sup>4</sup>

<sup>1</sup>Instituto de Parasitología y Biomedicina Lopez-Neyra

<sup>2</sup>Bioinformatics Unit, Instituto de Parasitología y Biomedicina “López-Neyra”

<sup>3</sup>University of Granada

<sup>4</sup>Consejo Superior de Investigaciones Científicas

June 24, 2021

## Abstract

Liver fibrosis induced by chronic hepatic injury remains as a major cause of morbidity and mortality worldwide. Identification of susceptibility/prognosis factors and new therapeutic tools for treating hepatic fibrotic disorders of various etiologies are urgent medical needs. Cortistatin is a neuropeptide with potent anti-inflammatory and anti-fibrotic activities in lung that binds to receptors that are expressed in liver fibroblasts and hepatic stellate cells. Here, we evaluated the capacity of cortistatin to regulate liver fibrosis. We initially found that hepatic expression of cortistatin inversely correlated with liver fibrosis grade in mice and humans with hepatic disorders. Cortistatin-deficient mice showed exacerbated signs of liver damage and fibrosis and increased mortality rates when challenged to hepatotoxic and cholestatic injury. Compared to wild-type mice, non-parenchymal liver cells isolated from cortistatin-deficient mice showed increased presence of cells with activated myofibroblast phenotypes and a differential genetic signature that is indicative of activated hepatic stellate cells and periportal fibroblasts and of myofibroblasts with active contractile apparatus. Cortistatin treatment reversed *in vivo* and *in vitro* these exaggerated fibrogenic phenotypes and protected from progression to severe liver fibrosis in response to hepatic injury. In conclusion, we identify cortistatin as an endogenous molecular break of liver fibrosis and its deficiency as a potential poor-prognosis marker for chronic hepatic disorders that course with fibrosis. Cortistatin-based therapies emerge as attractive strategies for ameliorating severe hepatic fibrosis.

## CORTISTATIN REGULATES FIBROSIS AND MYOFIBROBLAST ACTIVATION IN EXPERIMENTAL HEPATOTOXIC- AND CHOLESTATIC-INDUCED LIVER INJURY

Raquel Benitez<sup>1</sup>, Marta Caro<sup>1</sup>, Eduardo Andres-Leon<sup>1</sup>, Francisco O’Valle<sup>2</sup>, Mario Delgado<sup>1</sup>

<sup>1</sup>Institute of Parasitology and Biomedicine Lopez-Neyra, PT Salud, Granada, Spain

<sup>2</sup>Dept. of Pathology, School of Medicine, IBIMER and IBS-Granada, University of Granada, Spain

**Authors’ emails:** Raquel Benitez: [rbenitez@ipb.csic.es](mailto:rbenitez@ipb.csic.es); Marta Caro: [martacm@ipb.csic.es](mailto:martacm@ipb.csic.es); Eduardo Andres-Leon: [eduardo.andres@csic.es](mailto:eduardo.andres@csic.es); Francisco O’Valle: [fovalle@ugr.es](mailto:fovalle@ugr.es); Mario Delgado: [mdelgado@ipb.csic.es](mailto:mdelgado@ipb.csic.es)

**Corresponding author:** Mario Delgado, Institute of Parasitology and Biomedicine Lopez-Neyra IPBLN-CSIC, PT Salud, Granada, Spain. email: [mdelgado@ipb.csic.es](mailto:mdelgado@ipb.csic.es). ORCID: 0000-0003-1893-5982.

**Word count:** 4893, Introduction (493 words), Results (1360 words), Discussion (1041 words).

**Data availability.** The data supporting the findings of this study are available from the corresponding author. Raw fastq files for RNAseq are publicly available at Sequence Read Archive (SRA): PRJNA714069. Upregulated and downregulated DEGs (FDR p-value<0.05) between  $CST^{-/-}$  and  $CST^{+/+}$  HSCs are listed in Table S5.

**Acknowledgments.** We thank J. Campos-Salinas and A. Barroso (IPBLN-CSIC) for their assistance in designing PCR and RNAseq strategy, and L. de Lecea (Stanford University, CA, USA) for providing the  $CST^{-/-}$  mice to establish initially the colony of animals used in this study.

**Competing interests.** None declared.

**Funding.** This study was mainly supported by the Spanish Ministry of Science and Innovation (MICINN, grant SAF2015-67787-R). R.B. was recipient of FPI fellowship from MICINN and E.A-L. was recipient of postdoctoral fellowship from regional Andalusian Government.

**Author contributions.** R.B. conducted most of the experiments and analyzed all the data. M.C. carried out real-time PCRs. E.A-L. analysed RNAseq results and public human data bases. F.O’V. performed the histopathological studies. M.D. conceived and designed the study, conducted *in vivo* experimental models, analyzed the data and wrote the manuscript. All authors edited the manuscript.

**Ethic statement.** The experiments reported in this study followed the ethical guidelines for investigations of experimental animals approved by the Animal Care and Use board and the Ethical Committee of Spanish Council of Scientific Research and performed in accordance with the guidelines from Directive 2010/63/EU of the European Parliament on the protection of animals used for scientific purposes. Animal studies are reported in compliance with the ARRIVE guidelines and with the recommendations made by the *British Journal of Pharmacology* .

**Declaration of transparency and scientific rigour.** This Declaration acknowledges that this paper adheres to the principles for transparent reporting and scientific rigour of preclinical research as stated in the BJP guidelines for Design & Analysis, Immunoblotting and Immunochemistry and Animal Experimentation, and as recommended by funding agencies, publishers and other organizations engaged with supporting research.

**Abbreviations:** BDL: bile duct ligation; CST: cortistatin;  $CST^{+/+}$  : wild-type mice;  $CST^{+/-}$  : partially cortistatin-deficient mice;  $CST^{-/-}$  : totally cortistatin-deficient mice; CTGF: connective tissue growth factor; DEG: differentially expressed gene; ECM: extracellular matrix; FDR, false discovery rate; GFAP: glial fibrillary acidic protein; GO: gene ontology; H&E: hematoxylin and eosin; GHSR: growth hormone-secretagogue receptor; PF: periportal fibroblast; RNAseq: RNA sequencing; RPLP0: ribosomal protein lateral stalk subunit P0;  $\alpha$ SMA:  $\alpha$ -smooth muscle cell;sstr: somatostatin-receptor.

## Abstract

Liver fibrosis induced by chronic hepatic injury remains as a major cause of morbidity and mortality worldwide. Identification of susceptibility/prognosis factors and new therapeutic tools for treating hepatic fibrotic disorders of various etiologies are urgent medical needs. Cortistatin is a neuropeptide with potent anti-inflammatory and anti-fibrotic activities in lung that binds to receptors that are expressed in liver fibroblasts and hepatic stellate cells. Here, we evaluated the capacity of cortistatin to regulate liver fibrosis. We initially found that hepatic expression of cortistatin inversely correlated with liver fibrosis grade in mice and humans with hepatic disorders. Cortistatin-deficient mice showed exacerbated signs of liver damage and fibrosis and increased mortality rates when challenged to hepatotoxic and cholestatic injury. Compared to wild-type mice, non-parenchymal liver cells isolated from cortistatin-deficient mice showed increased presence of cells with activated myofibroblast phenotypes and a differential genetic signature that is indicative of activated hepatic stellate cells and periportal fibroblasts and of myofibroblasts with active contractile apparatus. Cortistatin treatment reversed *in vivo* and *in vitro* these exaggerated fibrogenic phenotypes and protected

from progression to severe liver fibrosis in response to hepatic injury. In conclusion, we identify cortistatin as an endogenous molecular break of liver fibrosis and its deficiency as a potential poor-prognosis marker for chronic hepatic disorders that course with fibrosis. Cortistatin-based therapies emerge as attractive strategies for ameliorating severe hepatic fibrosis.

**Key words:** neuropeptide, bile duct ligation, hepatic stellate cell, periportal fibroblast, contractile fibers.

**Lay summary:** Chronic liver fibrosis constitutes a serious public health issue for which safe and effective treatments are lacking. This study shows that the neuropeptide cortistatin acts as an endogenous break of hepatic fibrosis and an attractive therapeutic agent in preclinical models of liver damage of different etiologies. The anti-fibrotic effects of cortistatin are directly exerted by regulating the activation and differentiation of hepatic myofibroblasts.

### **Bullet Point Summary:**

#### *‘What is already known’*

-Development of chronic fibrosis is critical in the progression of cirrhosis and its associated complications in many hepatic disorders. -Myofibroblasts are the main pathological players in liver fibrogenic responses and urges the identification of factors that regulate their activation. -Cortistatin is a potent anti-inflammatory neuropeptide that downregulates acute fibrosis in lung.

#### *‘What this study adds’*

-The expression of cortistatin in human and mouse livers inversely correlates with the severity of fibrosis and cirrhosis. -Treatment with cortistatin ameliorates fibrosis progression and activation of myofibroblasts in two models of hepatotoxic and cholestatic liver injury. -Deficiency in cortistatin significantly exacerbates fibrogenic responses, hepatic damage and mortality. -We identify to cortistatin as an endogenous molecular break for the activation of hepatic stellate cells and fibroblasts and for the differentiation of myofibroblasts in liver.

#### *‘Clinical significance’*

-Deficiency in cortistatin could be further examined as a potential biomarker of susceptibility or poor-prognosis of developing severe hepatic fibrosis and cirrhosis. -Cortistatin-based therapies could serve for treating chronic hepatic disorders of different aetiologies to reduce disease severity and mortality.

### **INTRODUCTION**

Chronic tissue injury leads to fibrosis in various organs (1). In liver, development of fibrosis, resulting from a wound-healing response that has gone out of control after tissue injury, is the first step toward the progression of cirrhosis and the associated complications (2,3). During this pathological fibrotic response, newly activated/differentiated myofibroblasts, which are not present in normal liver, are responsible of the excessive extracellular matrix (ECM) deposition, formation of fibrous scar and tissue remodeling (1). Evidence indicates that the perisinusoidal hepatic stellate cells (HSCs) are the main sources of myofibroblasts in fibrotic liver (4-6). Upon fibrogenic activation (i.e., TGF $\beta$ 1), HSCs secrete fibrillary ECM components (type I and III collagens, fibronectin), express  $\alpha$ -smooth muscle actin ( $\alpha$ SMA) forming part of organized intracellular stress fibers and acquire contractile functions. Because formation of fibrous scar and activation/differentiation of ECM-producing myofibroblasts play central roles in the pathogenesis and progression of liver fibrosis, the identification of factors that limit or reverse these processes is critical for understanding the pathophysiology and identifying new therapeutic targets of several chronic hepatic disorders.

Cortistatin is a cyclic neuropeptide, initially discovered in brain cortex and hippocampus (7), which shows high-homology with somatostatin and recently emerged as a potent immunomodulatory agent (8). By regulating the production of inflammatory factors, cortistatin was able to indirectly impair fibrotic responses in various experimental models of inflammatory disorders, including sepsis, acute lung injury, myocarditis or inflammatory bowel disease (9-12), and its direct effect on pulmonary fibrogenic responses was recently

described (M.D., manuscript under consideration). Some data point-out to a potential anti-fibrotic action of cortistatin in liver. Thus, cortistatin-receptors (somatostatin-receptors sstr1-5 and ghrelin-receptor GHSR) are expressed in fibroblasts and HSCs, and various sstr/GHSR-agonists were described that exert anti-fibrotic responses in liver (13-20). Moreover, in several non-fibroblastic cells, cortistatin inhibited signaling pathways that are involved in fibrogenic responses (20-23). Finally, in a preliminary analysis of public data bases (24-26), we found that cortistatin expression is significantly reduced in human fibrotic or cirrhotic livers compared to normal liver tissue of healthy individuals. The inverse correlation that exists between human liver injury/fibrosis and cortistatin expression together with the capacity of cortistatin to potentially signal through various antifibrotic-linked receptors and intracellular pathways support the hypothesis that it could act as an endogenous regulator of hepatic fibrosis.

In this study, we investigated the potential protective role of cortistatin in the development of pathological liver fibrosis by using well-recognized experimental mouse models that mimic the two general types of chronic liver diseases, hepatocellular injury (such as chronic viral hepatitis, hepatotoxicity and nonalcoholic steatohepatitis) caused by repeated injections of the toxic agent carbon tetrachloride ( $\text{CCl}_4$ ), and cholestatic injury (such as primary biliary cirrhosis and sclerosing cholangitis) caused by common bile duct ligation (BDL). We induced both experimental models of chronic hepatic injury in wild-type and cortistatin-deficient mice and evaluated the progression of fibrosis as well as the therapeutic effect of exogenously administered cortistatin. We also investigated the phenotype and genetic signature showed by HSCs lacking cortistatin gene.

## METHODS

**Animals and ethic statement.** The experiments reported in this study followed the ethical guidelines for investigations of experimental animals approved by the Animal Care and Use board and the Ethical Committee of Spanish Council of Scientific Research and performed in accordance with the guidelines from Directive 2010/63/EU of the European Parliament on the protection of animals used for scientific purposes. Animal studies are reported in compliance with the ARRIVE v.2.0 guidelines (27) and with the recommendations made by the *British Journal of Pharmacology*. Mice lacking the gene for cortistatin ( $\text{CST}^{-/-}$ ) were a generous gift of Dr. Luis de Lecea (Stanford University, La Jolla, CA, USA) and were generated in a C57BL/6 background and backcrossed with C57BL/6 mice for ten generations as previously described (28). Mice heterozygous ( $\text{CST}^{+/-}$ ) for cortistatin were generated by crossing female  $\text{CST}^{-/-}$  and male  $\text{CST}^{+/+}$  mice.  $\text{CST}^{+/-}$  breeding pairs were used to generate a littermate colony of wild-type ( $\text{CST}^{+/+}$ ), heterozygous ( $\text{CST}^{+/-}$ ) and knockout ( $\text{CST}^{-/-}$ ) mice for cortistatin. Both male and female mice (20-24g body weight, 8-10 weeks-old) were used in all experiments described in this study, and no differences were found between sexes. All animals were housed in a controlled-temperature/humidity environment ( $22 \pm 1^\circ\text{C}$ , 60-70% relative humidity) in individual cages (10 mice per cage, with wood shaving bedding and nesting material), with a 12 h light/dark cycle (lights on at 7:00 a.m.) and fed with rodent chow (Global Diet 2018, Harlan) and tap water ad libitum. Mice were allowed to acclimatize to the experimental room for one hour before experiments. Mice were randomly assigned to the different experimental groups. Experiments were designed to make sample sizes relatively equal. However, this was not possible in some experiments due to the differential mortality rates occurring between genotypes and response to liver fibrosis. None of the animals were excluded from the study. Power calculations were performed using the software G\*Power ([www.gpower.hhu.de](http://www.gpower.hhu.de)) to ensure that adequate group sizes were used for the studies detailed below. For *in vivo* animal models, we calculated a minimum size of five to eight mice per group in order to have a power  $>0.95$  of detecting approximately a 30% change, assuming a standard deviation of 30% at a significance level of  $p < 0.05$ , expecting an effect size of 1.82 for ANOVA tests. In primary cell cultures, for effect sizes between 3.1 and 4, experiments were repeated at least four times to obtain  $p < 0.05$  and a power  $>0.95$ .

**Induction of experimental liver fibrosis.** To investigate the effect of cortistatin deficiency in severity of toxic hepatic fibrosis,  $\text{CST}^{+/+}$ ,  $\text{CST}^{+/-}$  and  $\text{CST}^{-/-}$  mice were injected i.p. with a low-dose of  $\text{CCl}_4$  (0.5  $\mu\text{l/g}$  body weight, dissolved at 1:9 in olive oil, twice/week, for six weeks). Mice injected with olive oil were used as controls of reference. To evaluate the therapeutic effect of cortistatin, hepatic fibrosis was induced in  $\text{CST}^{+/+}$  mice by i.p. injections of high-dose of  $\text{CCl}_4$  (0.5  $\mu\text{l/g}$ , dissolved at 1:3 in olive oil, twice/week, for six weeks)

and then treated i.p. with PBS or mouse cortistatin-29 (1 nmol/mouse, three times weekly, from Bachem, Bubendorf, Switzerland), starting 5 or 14 days after the first CCl<sub>4</sub> injection. Moreover, hepatotoxic fibrosis was induced in *CST*<sup>+/-</sup> and *CST*<sup>-/-</sup> mice with low-dose CCl<sub>4</sub> and immediately treated with cortistatin-29 (1 nmol/mouse, three times weekly).

To study the effect of cortistatin deficiency in cholestasis-induced hepatic fibrosis, anesthetized *CST*<sup>+/+</sup>, *CST*<sup>+/-</sup> and *CST*<sup>-/-</sup> mice were subjected to BDL as previously described (29). To investigate the therapeutic effect of cortistatin in BDL-induced fibrosis, *CST*<sup>+/+</sup> and *CST*<sup>+/-</sup> mice were injected i.p. with PBS or cortistatin-29 (1 nmol/mouse), three times weekly, starting one or five days after surgery, respectively.

In both models, survival was monitored daily, and on different times after BDL or initiation of CCl<sub>4</sub> injection, animals were sacrificed by CO<sub>2</sub> affixation, liver lobes were collected and analyzed for histopathological signs, immunofluorescence and fibrotic gene expression as described below. Collagen content in liver lobes was measured using the hydroxyproline assay as previously described (30), and bilirubin levels in serum were determined by using a colorimetric MAK126 assay kit (Sigma-Aldrich, San Louis, MO, USA).

**Isolation and culture of HSCs.** HSCs were isolated from *CST*<sup>+/+</sup> and *CST*<sup>-/-</sup> mice as described (29,31) using in vivo enzymatic digestion of liver by pronase-collagenase perfusion through portal vein followed by enrichment by centrifugation of non-parenchymal cell suspension through an 8% Nycodenz density gradient (Merk/Sigma). Enriched HSCs (pooled from six mice) were cultured in complete-DMEM (DMEM supplemented with 10% fetal bovine serum, 100 U/ml penicillin/streptomycin and 2 mM L-glutamine, all from Gibco/Thermo-Fisher, Waltham, MA, USA) in 75 cm<sup>2</sup>-Nunc flasks at 37°C/5% CO<sub>2</sub>. After six days in culture, HSCs were either subjected to RNA isolation for real-time qPCR and next-generation transcriptome sequencing (RNAseq) or seeded secondarily (at 10<sup>4</sup>) in glass-coverslips inserted in 24-well plates and incubated for 24h or 96h in complete-DMEM for immunofluorescence analysis as described below. Cortistatin-29 was added (10 nM, every other day, for one week) during the primary 6 day-culture to study its capacity to reverse the observed phenotype.

**Analysis of gene expression of cortistatin in human fibrotic livers.** The levels of cortistatin gene expression were obtained from the National Cancer for Biotechnology Information Gene Expression Omnibus database based on the gene chips of fibrotic liver tissues associated to hepatitis B (HBV-GSE84044, ref. 24), hepatitis C-induced hepatocarcinoma (HCV-GSE14323, ref. 25), and nonalcoholic fatty liver disease (NAFLD-GSE49541, ref. 26). In HBV, 10 healthy samples (Scheuer stage S0/G0) were compared with 10 age-matched liver samples showing high fibrosis signs (Scheuer's stage S4). In HCV, 19 healthy samples were compared with 41 pre-malignant cirrhotic samples. In NAFLD, 40 samples showing mild stage were compared with 32 samples showing advanced stage. The raw data (Affymetrix U133A array) were processed together by correcting the background and normalizing the expression values through the rma function of the affy Bioconductor package (32).

**Histopathological analysis of liver fibrosis.** For histopathologic evaluation, freshly collected liver lobes were fixed in 10% buffered-formalin, paraffin-embedded and sectioned. Cross-sections (4-µm) were stained with hematoxylin/eosin (H&E) or Picosirius Red using standard techniques. Images were acquired in an Axio Scope.A1 microscope (Carl Zeiss, Germany). Histopathological analysis was performed in a blinded manner in whole liver sections. The extent of fibrosis was calculated as a percentage of Sirius red-positive area of the total section area (excluding the Glisson capsule from quantification) by using the thresholding method in the green channel of Fiji-ImageJ software (<http://imagej.net/Fiji>). Toxic-induced hepatic fibrosis was also quantified using a semi-quantitative Ishak-modified scale from 0 (no fibrosis) to 4 (fibrous expansion of portal areas with marked portal-to-portal and portal-central bridging) as described (33,34). BDL-induced hepatic damage was also determined by quantifying the percentage of necrotic area in H&E-stained liver sections using Fiji-ImageJ software. Results show the mean value of 10 randomly selected areas per section and four sections per mouse.

**Immunofluorescence analysis.** Formalin-fixed liver sections were antigen-retrieved with 10 nM sodium citrate/0.05% Tween-20 (20 min/95°C), blocked with 10% goat serum/1% bovine serum albumin (BSA,

2h/20°C) and marked with primary mouse anti-mouse  $\alpha$ SMA antibody (dilution 1:1000 in PBS/1% BSA, 8h/4°C), and subsequently with secondary Alexa Fluor 488-goat anti-mouse IgG antibody (1:1000, 1h/20°C). See table S6 for antibodies' information. Nuclei were DAPI-counterstained (Sigma-Aldrich, 1:1000, 5 min/20°C). Samples in which primary antibody was omitted were used as negative controls. Sections were examined in an Olympus iX81 fluorescence microscope (Olympus Life Science, Hamburg, Germany) and the images were acquired (Olympus CellSens Imaging software) using the same parameters between samples. The percentage of  $\alpha$ SMA-positive area was quantified using the Fiji-ImageJ software (10 areas/section, two sections/mouse).

HSCs cultured in coverslips as above were fixed with 4% paraformaldehyde/2% glucose (15 min/20°C), blocked with 30 mM glycine (5 min/20°C) and PBS/5% BSA/0.3% Triton X-100 (1h/20°C) and marked with primary mouse anti-mouse  $\alpha$ SMA (1:1000, in PBS/1% BSA/0.3% Triton X-100, 8h/4°C) and rabbit anti-mouse glial fibrillary acidic protein (GFAP, 1:300, 8h/4°C) antibodies, and then with secondary Alexa Fluor 488-donkey anti-rabbit IgG and Alexa Fluor 594-goat anti-mouse IgG antibodies (1:1000 in PBS/1% BSA/0.1% Triton X-100, 1h/20°C). Nuclei were DAPI-counterstained and images were acquired as described above.

**Gene expression analysis by real-time PCR.** RNA was isolated from liver by homogenization in Tri-Pure (Roche, Basilea, Switzerland) and from HSCs by lysis in EZNA HP Total RNA Kit (Omega Bio-Tek, Norcross, GA, USA) and treated with DNase 1 (Sigma-Aldrich) before reverse transcription (RevertAid First Strand cDNA Synthesis Kit, Thermo-Fisher) using random hexamers. SYBER green quantitative PCR (SensiFast Sybr No-Rox mix, Bioline, Germany) was performed on thermocycler (CFX96, Bio-Rad, Hercules, CA, USA) using the following conditions: 5 min/94°C followed by 40 cycles at 94°C/30 sec, 60°C/30 sec and 72°C/30 sec (primers' sequences are listed in table S7). The expression of each gene was normalized against the housekeeping gene RPLP0 in every PCR reaction and fold-change expression was estimated with Delta-Delta Ct method.

**Next-generation transcriptome sequencing (RNAseq).** RNA (1 $\mu$ g) from primary  $CST^{-/-}$  and  $CST^{+/+}$  HSC cultures (two independent biological replicated experiments each, with RNA Integrity Number coefficients >9, using Bioanalyzer RNA 6000 Nano-chip, from Agilent, Santa Clara, CA, USA) was used to prepare mRNA libraries with TruSeq Stranded mRNA Library Prep Kit (Illumina, San Diego, CA, USA). Quality and size distributions of indexed mRNA libraries were validated by Bioanalyzer High Sensitivity DNA assay (Agilent) and the final libraries were pooled equimolecularly and diluted/denatured as recommended. The 40x2nt paired-end sequencing was conducted on an Illumina NextSeq-500 sequencer (highest output mode), producing 46,850,000 raw paired-reads on average. We used the miARma-Seq pipeline to analyze and calculate the differential expressed genes (DEGs) (35), with *Mus musculus* Gencode version M25 genome-build (mmGRCm38.p6) for alignment of reads. Differential expression analysis was conducted by using edgeR package (36) and genes were normalized by trimmed mean of M-values method (37). We calculated reads per kb per million mapped reads and log<sub>2</sub>-counts per million per gene in each sample (36). To infer the replicability/similarity of RNA-sequencing samples, we used Principal Component analysis and Hierarchical Clustering of normalized samples (38,39). Genes giving False Discovery Rate (FDR) values <0.05 were marked as DEGs and Log<sub>2</sub>-FC was used to calculate the fold-change expression of each gene between  $CST^{-/-}$  HSCs and  $CST^{+/+}$  HSCs. To identify the effects of DEGs, functional enrichment study was carried out using the clusterProfiler Bioconductor package (40), in which DEGs were compared against all expressed genes in the RNA-seq assay. Gene Ontology (GO) terms (Biological process, Molecular function, Cellular components) were obtained from the Bioconductor *Mus musculus* database and associated to Entrez gene identifiers in an *orgDB* R object through the AnnotationForge package (with clusterProfiler).

**LX2 cell culture.** The human HSC line *LX2* was obtained from Merck Millipore (Burlington, MA, USA, Cat. #SCC064) and maintained in complete DMEM medium (DMEM supplemented with 10% fetal bovine serum and 1% penicillin/streptomycin, all from Gibco/Thermo-Fisher) at 37°C and 5% CO<sub>2</sub>.

To determine the effect of cortistatin in protein and gene expression of fibrotic markers, 0.7-1 x 10<sup>5</sup> *LX2* cells were cultured in 25 cm<sup>2</sup>-Nunc flasks (for protein expression) or in 6-well-Nunc plates (for gene expression)

in complete DMEM medium for 24h (for protein) or until reach confluence of 70-80% (for gene). Cells were synchronized overnight with incomplete serum-free DMEM (supplemented with 1% penicillin/streptomycin) and then cultured in complete DMEM in the absence (unstimulated) or presence of TGF $\beta$ 1 (5 ng/ml, from PeproTech, London, UK), with or without human cortistatin-17 (100 nM, added every 48h, from Bachem). When indicated, the pan-antagonist for sstr1-5 cyclosomatostatin (at 1  $\mu$ M, Sigma-Aldrich), the specific GHSR1-antagonist GHRP6 (at 1  $\mu$ M, Sigma-Aldrich) and the protein kinase A inhibitor H89 (at 100 nM, Sigma-Aldrich) were added to cultures simultaneously to cortistatin, and the G $\alpha$ i-inhibitor pertussis toxin (at 250 ng/ml, Sigma-Aldrich) was administered during the phase of *LX2* synchronization. After 24h or 7d of culture, cells were lysed and protein extracts and analyzed as described below and total RNA were isolated with TriPure and analyzed by real-time qPCR as described for liver and HSCs.

To determine the effect of cortistatin in the presence of intracellular  $\alpha$ SMA in activated *LX2*,  $5 \times 10^4$  cells were plated on glass-coverslips inserted in 24-well-Nunc plates and incubated in complete DMEM until reach 70% confluence. *LX2* cells were synchronized overnight and then stimulated in complete DMEM with TGF $\beta$ 1 (5 ng/ml) in the absence or presence of human cortistatin-17 (100 nM, added every 48h). After 7 days of culture, immunofluorescence analysis was conducted as described below.

**Western blot analysis of *LX2* cultures.** *LX2* cells were cultured and activated as described above and then lysed by incubation with lysis buffer containing 50 mM Tris-HCl pH 7.8, 150 mM NaCl, 1 mM EDTA, 1% Triton X-100, 1% sodium deoxycholic acid, 0.1% SDS, 10  $\mu$ g/ml<sup>-1</sup> protease inhibitor cocktail (Sigma-Aldrich, cat#P8465) and phosphatase inhibitor (PhosSTOP, from Roche) for 2h at 4°C and shaking. Lysates were centrifuged (21,000xg, 15 min, 4°C) and supernatants containing proteins extracts (20  $\mu$ g) were separated on 12% SDS-polyacrylamide gels and blotted onto polyvinylidene difluoride membranes (ImmMobilon-FL PVDF, Millipore) using a semidry system (transfer buffer: 25 mM pH 8.3, 192 mM glycine, 20% methanol). Membranes were blocked with TBS-T buffer (10 mM Tris, 150 mM NaCl, pH 7.5, 0.1% Tween-20) and 5% BSA for 1h at 20°C and subsequently probed overnight at 4°C with pairs of primary rabbit anti-human CTGF or rabbit anti-human  $\alpha$ SMA antibodies (both diluted at 1:1,000 in TBS-T/2% BSA) and mouse anti-human  $\alpha$ -tubulin antibody (diluted at 1:8,000). Immunodetection of primary antibodies was performed by incubation with secondary antibodies labelled to the near-infrared fluorophores: goat anti-rabbit IRDye 800CW (green dye, for CTGF and  $\alpha$ SMA) or goat anti-mouse IRDye 680RD (red dye, for  $\alpha$ -tubulin) diluted at 1:20,000 in TBS-T/2% BSA/0.02% SDS for 1h at 20°C. Images of blots were acquired in an Odyssey CLX (LI-COR Biosciences, Lincoln, NE, USA) and fluorescence intensities of specific bands corresponding to CTGF,  $\alpha$ SMA or  $\alpha$ -tubulin (used to normalize protein expression) were quantified using Fiji-ImageJ software.

**Immunofluorescence analysis of *LX2* cultures.** *LX2* cells were cultured in coverslips as described above and then fixed with 4% paraformaldehyde/2% glucose during 15 min at 20°C. After extensive washing with PBS, cells were incubated with 30 mM glycine for 5 min (to reduce autofluorescence), permeabilized with 0.1% Triton X-100 (15 min, 20°C), and blocked with PBS/5% FBS/0.3% Triton X-100 (60 min, 20°C). Cells were then incubated with primary anti-human  $\alpha$ SMA monoclonal antibody diluted at 1:1,000 in PBS/1% BSA/0.3% Triton X-100 at 4°C for 8h. After extensive washing with PBS/0.025% Triton X-100, samples were incubated with secondary Alexa Fluor 488-conjugated goat anti-mouse IgG antibody (60 min, 20°C, diluted at 1:1,000 in PBS/1% BSA/0.1% Triton X-100). Nuclei were DAPI-counterstained (1:500 in PBS, 5 min, 20°C) and were mounted in Mowiol. Samples in which we omitted the primary antibodies were used as negative controls, showing in all cases lack of fluorescence signal. Samples were examined in an Olympus IX81 fluorescence microscope and the images acquired at 400X magnification (Olympus CellSens Imaging software) using the same parameters and ROI of at least eight independent experiments and fluorescence intensity and area were determined using the Fiji-ImageJ software.

**Data and statistical analysis.** All experiments are randomized and blinded. All data are expressed as mean $\pm$ SEM. To control for unwanted sources of variation between individual experiments, data obtained from qPCR and western blot analysis of *LX2* cell cultures were normalized to the mean of unstimulated cells. No data were excluded and outliers were included in data analysis and presentation. Group size is the number of

independent animals or cell cultures, and statistical analysis was performed using these independent values. The data and statistical analysis comply with the recommendations on experimental design and analysis in pharmacology (41). In accordance with journal policy, statistical analysis was performed only when a minimum of  $n = 5$  independent samples was acquired. We analysed data for statistical differences between groups using the unpaired Student's t-test or the non-parametric Mann-Whitney U-test and, if appropriate, by Kruskal-Wallis analysis of variance test. Survival curves were analysed by the Kaplan-Meier log-rank test. All analyses were performed using GraphPad Prism v5.0 software (La Jolla, CA, USA). We considered P-values  $< 0.05$  (two-tailed) as significant.

## RESULTS

**Cortistatin is downregulated in fibrotic livers.** We first analyzed the expression of cortistatin in livers from mice subjected to experimental induction of hepatic fibrosis and from patients with different hepatic fibrosis disorders. The levels of cortistatin gene expression were obtained from the National Cancer for Biotechnology Information Gene Expression Omnibus database based on the gene chips of fibrotic liver tissues associated to hepatitis B virus (HBV-GSE84044, ref. 24), hepatitis C virus-induced hepatocarcinoma (HCV-GSE14323, ref. 25), and nonalcoholic fatty liver disease (NAFLD-GSE49541, ref. 26). We found that cortistatin expression is significantly reduced in fibrotic or cirrhotic livers of these patients compared to normal liver tissue of healthy individuals (Fig. 1A). This inverse correlation between cortistatin expression and human fibrosis was also observed in livers isolated from mice subjected to hepatic fibrosis by intoxication with  $\text{CCl}_4$  or by cholestasis (Fig. 1B).

**Deficiency in cortistatin exacerbates fibrosis caused by cholestatic and toxic-induced hepatic injury.** To investigate whether a deficiency in cortistatin predisposes to suffer exacerbated hepatic fibrosis, we induced experimentally chronic liver injury by  $\text{CCl}_4$ -intoxication or by BDL-induced cholestasis in mice that partially ( $CST^{+/-}$ ) or totally ( $CST^{-/-}$ ) lack the cortistatin gene, and the progression and severity of the fibrotic disease were compared with those observed in wild-type mice ( $CST^{+/+}$ ). We initially observed that in the absence of hepatic insults, cortistatin-deficient mice did not show marked signs of liver fibrosis, although dispersed incipient inflammatory/fibrotic foci were more abundant in livers of sham-operated or vehicle-injected  $CST^{+/-}$  or  $CST^{-/-}$  mice than of wild-type animals (fig. S1). Interestingly, whereas BDL did not affect the survival of wild-type mice, it resulted in mortality rates around 40% in cortistatin-deficient mice (Fig. 2A). Histopathological examination of Sirius red-stained liver sections showed that  $CST^{+/-}$  and  $CST^{-/-}$  mice had larger areas of fibrosis compared to  $CST^{+/+}$  mice (Fig. 2B), which correlated with excessive hepatic damage, as assessed by increased necrotic area (Fig. 2C, fig. S2A) and bilirubin levels (Fig. 2D). Development of severe liver fibrosis in cortistatin-deficient mice subjected to BDL was associated with enhanced presence of  $\alpha\text{SMA}^+$ -activated myofibroblasts in periportal areas and fibrotic portal-to-portal branches (Fig. 2E), excessive collagen content (Fig. 2F) and increased mRNA expression of critical fibrogenic markers, including TGF $\beta$ 1, collagen I- $\alpha$ 2 (Col1a2), connective-tissue growth factor (CTGF) and  $\alpha\text{SMA}$  (Fig. 2G).

On the other hand, chronic injection of a low dose of  $\text{CCl}_4$  elevated the mortality rate to 25% in cortistatin-deficient mice (Fig. 3A), which correlated with a significant early and exacerbated progressive liver fibrosis, characterized by increased Sirius red<sup>+</sup>-areas in most of portal spaces, with occasional portal-to-portal bridging (corresponding to Ishak score of 3) and enlargement of Glisson capsule (Fig. 3B, fig. S2B). Moreover, we observed elevated presence of  $\alpha\text{SMA}^+$ -myofibroblasts and contents of bilirubin and hepatic collagen, and excessive expression of profibrogenic factors in  $CST^{+/-}$  and  $CST^{-/-}$  mice compared to wild-type mice (Fig. 3C-E). Interestingly, necropsy of cortistatin-deficient mice that died as consequence of chronic  $\text{CCl}_4$ -exposition showed the occurrence of damaged lungs, and histopathological analysis confirmed the presence of extended edematous and hemorrhagic foci with distortion of pulmonary structure (fig. S3).

All together, these findings indicate that cortistatin is a key regulator of pathological fibrosis induced by chronic hepatic injury, acting as a protective anti-fibrotic factor that limits the activation/differentiation of myofibroblasts.

**Cortistatin-deficient HSCs show exacerbated fibrotic responses and excessive differentiation**

**capacity to activated myofibroblasts.** Numerous evidences demonstrate that pathological fibrosis in liver is driven by differentiated myofibroblasts and that the major contributors of the myofibroblast pool are liver resident activated perisinusoidal HSCs and periportal fibroblasts (PF) (4-6). In order to investigate whether endogenous cortistatin directly regulates these profibrogenic cells, we evaluated the phenotype and fibrogenic responses of the nonparenchymal cell fraction (enriched in HSCs) isolated from livers of wild-type and cortistatin-deficient mice and then cultured as described in Fig. 4A. We first confirmed the expression of cortistatin by mouse HSCs (fig. S4A). After one week in culture, most of the wild-type nonparenchymal cells (>80%) displayed a quiescent/non-activated HSC phenotype (GFAP<sup>+</sup>/αSMA<sup>-</sup>), and less than 10% of them corresponded to activated myofibroblasts expressing αSMA<sup>high</sup>-stress fibers (Fig. 4B). However, cortistatin-deficient HSC cultures showed initially a significant elevated percentage (>30%) of activated αSMA<sup>high</sup>-myofibroblasts that progressed rapidly to more than 70% of total cells at the end of culture, a percentage that was largely higher than that observed (<30%) in *CST*<sup>+/+</sup> HSC cultures (Fig. 4B). Moreover, *CST*<sup>-/-</sup> HSC cultures showed 1.8-fold cell numbers than *CST*<sup>+/+</sup> HSC cultures. The enhanced fibrogenic/myofibroblastic phenotype observed in *CST*<sup>-/-</sup> HSCs correlated with an initial increased expression of profibrotic markers/mediators compared to *CST*<sup>+/+</sup> HSCs (Fig. 4C), suggesting that cortistatin-deficient HSCs are more committed than wild-type HSCs to differentiate to activated myofibroblasts.

To further investigate the genetic profile/signature that could be associated to this commitment, we compared the transcriptomes of *CST*<sup>+/+</sup> and *CST*<sup>-/-</sup> HSCs by using next-generation RNAseq. We observed that 2,289 genes (1,284 upregulated and 1,005 downregulated) displayed significant differential expression (FDR p-value<0.05) in cortistatin-deficient HSCs compared to wild-type HSCs (Fig. 4D). The expression of selected upregulated and downregulated genes of the RNAseq were validated by real-time PCR, showing a high-degree of correlation between both analyses (fig. S4B). The unsupervised hierarchical clustering analysis of the most significant differentially expressed genes (DEGs) revealed two distinct groups with minimal overlap (Fig. 4E). Interestingly, we observed that from the top-25 annotated DEGs that are upregulated in *CST*<sup>-/-</sup> HSCs, 22 corresponded to genes related specifically to differentiation/generation, function or markers of muscle cells (Fig. 4F, table S1), and that 53 muscle-related genes were increased at least four-fold in cortistatin-deficient HSCs (fig. S4C). Further, the gene ontology (GO) analysis revealed that the DEGs (mostly upregulated) were mainly associated with biological functions or terms that are related to muscle function, myofibroblast activation/differentiation and extracellular matrix deposition (Fig. 4G, tables S2 to S4). Interestingly, a significant number of downregulated DEGs in *CST*<sup>-/-</sup> HSCs are associated with GO terms that are related to defense response, mainly to interferon and viral infection (Fig. 4G, table S3). Moreover, a detailed analysis of DEGs showed that specific markers of activated HSCs and PF were upregulated in nonparenchymal liver cells isolated from cortistatin-deficient mice (fig. S4, D and E). In addition, several inhibitors of HSC senescence were increased in *CST*<sup>-/-</sup> HSCs (fig. S4F). These findings suggest that cortistatin could act as an endogenous break of fibroblast and HSC activation and of their differentiation to activated myofibroblasts with potential contractibility. In fact, the addition of exogenous cortistatin to *CST*<sup>-/-</sup> HSC cultures reversed significantly this activated myofibroblastic phenotype (Fig. 4H).

To confirm that cortistatin directly downregulates HSC function, we investigated its effect on *LX2* cells, a widely used human HSC line to study fibrogenic responses (42). We observed that cortistatin impaired the activation in TGFβ1-stimulated *LX2* cells (fig. S5, A to C). Interestingly, the inhibitory effects of cortistatin in *LX2* cells were partially blocked by antagonists for sstr and GHSR1, and by inhibiting Gαi and protein kinase A, two signaling factors that are coupled both receptors (fig. S5D). This supports the involvement of sstr and GHSR in the anti-fibrotic activity of cortistatin in HSCs. As occurred in mouse samples, *LX2* cells constitutively expressed cortistatin, which was downregulated upon fibrogenic stimulation (fig. S5E). These results are the first insights to potentially translate our observations in preclinical models to humans.

### **Treatment with cortistatin ameliorates fibrosis induced by toxic and cholestatic liver injury.**

Our previous results indicate that cortistatin has a critical role in the regulation of hepatic fibrosis and that administration of cortistatin is a potential strategy for the prevention and treatment of liver injury. First, we found that systemic injection of cortistatin reversed the exacerbated fibrosis and hepatic damage observed in cortistatin-deficient mice subject to surgical BDL (Fig. 5) or to chronic injection of low-dose

CCl<sub>4</sub> (fig. S6). Moreover, treatment with cortistatin protected significantly against severe fibrosis and hepatic damage caused by chronic intoxication with high-dose CCl<sub>4</sub> (Fig. 6). Interestingly, the therapeutic effect of cortistatin was observed following both early (from day 5) and delayed (from day 14) regimes, pointing to a wide interventional therapeutic window (Fig. 6). Similarly, cortistatin treatment protected from development of cholestatic-induced hepatic fibrosis (fig. S7). These results suggest that cortistatin-based therapies could avoid the progression to severe hepatic fibrosis in susceptible individuals and attenuate the established liver fibrosis.

## DISCUSSION

Although wound-healing is a physiological process aimed at restoring normal tissue structure and function after an injury, it can be more damaging than the insult itself if becomes uncontrolled and excessive (1). In the liver, a dysregulated fibrotic response to tissue injury of various etiologies, including viral infections, toxics, biliary obstruction and nonalcoholic steatohepatitis, occurs and is associated to poor prognosis in several of the chronic hepatic disorders with elevated incidence, morbidity and mortality worldwide (2,3). Evidence indicates that a precise balance between fibrogenic and anti-fibrotic factors must exist to tune adequately the wound-healing response (43). By using two well-characterized experimental models of chronic liver fibrosis, we here recognize cortistatin as an endogenous protective factor. We found that a deficiency in cortistatin predisposes for developing exacerbated fibrotic responses in injured livers after exposition to hepatotoxic compounds, even at low doses, or after cholestatic damage, and to suffer subsequently more severe clinical signs, hepatic damage and increased mortality. Hallmarks of the exacerbated fibrogenic responses observed in injured livers of cortistatin-deficient mice included the excessive occurrence of portal-to-portal fibrous scars, ECM-deposition and activated myofibroblasts.

Our data indicate that cortistatin could acts as an endogenous negative regulator in the activation and/or differentiation of myofibroblast, a major player in the development of pathological hepatic fibrosis (44). Non-parenchymal cells isolated from livers of cortistatin-deficient mice showed excessive presence of cells compatible with an activated myofibroblast phenotype (45,46) characterized by enhanced expression of intracellular  $\alpha$ SMA<sup>+</sup>-stress fibers and production of fibrogenic markers. In agreement with this commitment to myofibroblastic differentiation, the genetic signature of the cortistatin-deficient hepatic non-parenchymal cells displayed increased expression of a significant number genes related to collagen-containing ECM secretion, fiber formation and focal adhesion, but mainly, linked to function and development of muscle, actin cytoskeleton and contractile cellular fibers, including many components of muscular myosin complexes. Moreover, whereas genes, such as myogenin, myomarker (Mymk) and myogenic differentiation 1 (Myod1) that are involved in muscle differentiation/formation, are highly upregulated in cortistatin-deficient cells, the expression of myostatin, a gene that blocks myogenesis, was significantly decreased. This muscle-like phenotype is supported by the fact that cortistatin-deficient cells expressed genes encoding for delta and gamma subunits of cholinergic/nicotinic-receptors, which are solely expressed in muscle cells, which are almost 200-fold upregulated, but did not differentially express other cholinergic-receptor subunits that are present in other cells. Similarly, the gene encoding the muscle-specific carbonic anhydrase isoform Car3, but not other isoforms, was differentially increased (40-fold) in cortistatin-deficient cells. These findings suggest that lack of cortistatin in non-parenchymal hepatic cells favors the generation of myofibroblasts with contractile functions, and treatment with cortistatin impairs their differentiation. This entails important pathological consequences, because contractile myofibroblasts are abundant in the advanced phases of liver fibrotic disorders and are highly resistant to reversion/resolution of the fibrogenic response (47,48).

Numerous evidences support that HSCs are the major sources for activated myofibroblasts (4-6,49). However, several studies demonstrated that other fibrogenic cells could also contribute to myofibroblast generation depending of liver damage etiology (4-6). Whereas fibrosis in hepatotoxic liver injury is attributed to activated HSCs, activated PFs are implicated in liver fibrosis caused by cholestatic liver injury (4-6,49). Our and other studies showed that cortistatin and its receptors are expressed in HSCs and PFs, and therefore, it could act in both fibrogenic cells in an autocrine/paracrine manner (14,18,20). In fact, treatment with cortistatin reversed the activated myofibroblastic phenotype observed in cortistatin-deficient hepatic cells,

and impaired the activation of human cell line of HSCs, pointing to these cells as major targets for the anti-fibrotic effect of cortistatin. Moreover, we observed that non-parenchymal liver cells lacking cortistatin showed significant increased expression of genes that are specifically associated to activated HSCs. However, deficiency in cortistatin also enhanced the levels of genes that are mostly expressed in activated PFs. Therefore, cortistatin could act as an endogenous break of activated HSCs and PFs and of their differentiation to activated myofibroblasts, and consequently, as a critical protective factor for developing severe liver fibrosis, independently of the hepatic injury type. Despite this direct effect on fibrogenic hepatic cells, we cannot fully discard the anti-inflammatory activity of cortistatin as an indirect additional mechanism involved in its anti-fibrotic effect in vivo, because inflammation is a major driver of fibrosis in many organs, including liver. However, the fact that cortistatin treatment efficiently reduced hepatic fibrosis when initiated once that the inflammatory response was fully established also supports the capacity of cortistatin to directly limit fibrogenic responses in injured livers.

Our findings have several clinical implications both from diagnostic and therapeutic points of view. The fact that a simple partial deficiency in cortistatin could predispose for developing exacerbated fibrotic responses could be used to anticipate the diagnostic of more severe forms of chronic hepatic disorders. Indeed, we found an inverse correlation between hepatic cortistatin levels and fibrosis/cirrhosis in patients and animals with different types of liver damage, and it will be intriguing corroborating these findings in plasma of patients to consider cortistatin as a potential biomarker of disease prognosis and susceptibility. The deficiency in cortistatin, and therefore the susceptibility to suffer exacerbated fibrosis, could be circumstantial and more or less transitory (i.e., chronic stress, sleep-deprivation) or permanent (i.e., individuals with 1p36 monosomy, the most common subtelomeric terminal-deletion syndrome, which are heterozygous for cortistatin) (50,51). In any case, our study demonstrates that a systemic cortistatin-based treatment would correct easily this deficiency and improve disease progression. Noteworthy is that cortistatin-treatment has a favorable safety profile in humans and demonstrated clinical efficacy in Cushing's disease (52), and that the interest of pharmaceutical industry in developing cortistatin-based analogues with improved half-life in serum and clinical efficiency has increased lately (53). Previous studies described the therapeutic effect on fibrogenic responses by various agonists that signal through receptors that are recognized by cortistatin, including sstr and GHSR (13-20), suggesting that binding of cortistatin to both receptor-classes could allow a kind of synergic anti-fibrotic effect in liver, a hypothesis that is confirmed here in activated *LX2* cells.

In summary, this study provides new insights into the protective function of cortistatin in liver fibrosis, acting as an endogenous break of activation/differentiation of myofibroblasts. Beside as a potential biomarker of disease susceptibility/protection, cortistatin emerges as an attractive candidate for designing anti-fibrotic therapies to treat chronic hepatic disorders of different etiologies.

#### LIST OF SUPPLEMENTARY MATERIAL

- Fig. S1. Effects of deficiency in cortistatin in liver histology of naïve, sham-operated and vehicle-treated mice.
- Fig. S2. Histopathological signs of exacerbated hepatic fibrosis in cortistatin-deficient mice.
- Fig. S3. Lung pathology accompanied exacerbated hepatic fibrosis in cortistatin-deficient mice.
- Fig. S4. Cortistatin-deficient hepatic stellate cells (HSCs) show exacerbated myofibroblastic responses.
- Fig. S5. Cortistatin regulates activation of human HSC *LX2*line.
- Fig. S6. Treatment with cortistatin reversed the exacerbated toxic-induced liver fibrosis observed in cortistatin-deficient mice.
- Fig. S7. Exogenous administration of cortistatin protects from cholestatic-induced hepatic fibrosis.
- Table S1. List of muscle-related genes found within the Top-25 upregulated differentially expressed genes (DEGs) in *CST*<sup>-/-</sup> HSCs (ordered by fold-change expression).

- Tables S2. Annotated differentially expressed genes (DEGs) in Gene Ontology (GO) terms for Cellular Components for  $CST^{-/-}$  HSCs versus  $CST^{+/+}$  HSCs.

Tables S3. Annotated differentially expressed genes (DEGs) in Gene Ontology (GO) terms for Body Processes for  $CST^{-/-}$  HSCs versus  $CST^{+/+}$  HSCs.

Tables S4. Annotated differentially expressed genes (DEGs) in Gene Ontology (GO) terms for Molecular Functions for  $CST^{-/-}$  HSCs versus  $CST^{+/+}$  HSCs.

- Table S5. Annotated differentially expressed genes (DEGs) in Gene Ontology (GO) terms for Molecular Functions for  $CST^{-/-}$  HSCs versus  $CST^{+/+}$  HSCs.

- Table S6. Antibodies used in the study.

- Table S7. Primer sequences for real-time qPCR analysis.

- Supplementary References.

## REFERENCES

1. Rockey DC, Bell PD, Hill JA. Fibrosis—a common pathway to organ injury and failure. *N Engl J Med* 2015;372:1138-1149.
2. Bataller R, Brenner DA. Liver fibrosis. *J Clin Invest* 2005;115:209-218.
3. Blachier M, Leleu H, Peck-Radosavljevic M, Valla DC, Roudot-Thoraval F. The burden of liver disease in Europe: A review of available epidemiological data. *J Hepatol* 2013;58:593-608.
4. Mederacke I, Hsu CC, Troeger JS, Huebener P, Mu X, Dapito DH, et al. Fate tracing reveals hepatic stellate cells as dominant contributors to liver fibrosis independent of its aetiology. *Nat Commun* 2013;4:2823.
5. Iwaisako K, Jiang C, Zhang M, Cong M, Moore-Morris TJ, Park TJ, et al. Origin of myofibroblasts in the fibrotic liver in mice. *Proc Natl Acad Sci USA* 2014;111:E3297-E3305.
6. Kisseleva T. The origin of fibrogenic myofibroblasts in fibrotic liver. *Hepatology* 2017;65:1039-1043.
7. de Lecea L, Criado JR, Prospero-Garcia O, Gautvik KM, Schweitzer P, Danielson PE, et al. A cortical neuropeptide with neuronal depressant and sleep-modulating properties. *Nature* 1996;381:242-245.
8. Gonzalez-Rey E, Delgado M. Emergence of cortistatin as a new immunomodulatory factor with therapeutic potential in immune disorders. *Mol Cell Endocrinol* 2008;286:135-40.
9. Gonzalez-Rey E, Chorny A, Robledo G, Delgado M. Cortistatin, a new antiinflammatory peptide with therapeutic effect on lethal endotoxemia. *J Exp Med* 2006;203:563-571.
10. Delgado-Maroto V, Falo CP, Forte-Lago I, Adan N, Morell M, Maganto-Garcia E, et al. The neuropeptide cortistatin attenuates experimental autoimmune myocarditis via inhibition of cardiomyogenic T cell-driven inflammatory responses. *Br J Pharmacol* 2017;174:267-280.
11. Gonzalez-Rey E, Chorny A, Del Moral RG, Varela N, Delgado M. Therapeutic effect of cortistatin on experimental arthritis by downregulating inflammatory and Th1 responses. *Ann Rheum Dis* 2007;66:582-588.
12. Gonzalez-Rey E, Varela N, Sheibanie AF, Chorny A, Ganea D, Delgado M. Cortistatin, an antiinflammatory peptide with therapeutic action in inflammatory bowel disease. *Proc Natl Acad Sci USA* 2006;103:4228-4233.
13. Tracy TF, Tector AJ, Goerke ME, Kitchen S, Lagunoff D. Somatostatin analogue (Octreotide) inhibits bile duct epithelial cell proliferation and fibrosis after extrahepatic biliary obstruction. *Am J Pathol* 1993;143:1574-1578.
14. Moreno M, Chaves JF, Sancho-Bru P, Ramalho F, Ramalho LN, Mansego ML, et al. Ghrelin attenuates hepatocellular injury and liver fibrogenesis in rodents and influences fibrosis progression in humans. *Hepatology* 2010;51:974-985.
15. Sikiric P, Seiwerth S, Grabarevic Z, Rucman R, Petek M, Rotkvic I, et al. Hepatoprotective effect of BPC 157, a 15-amino acid peptide, on liver lesions induced by either restraint stress or bile duct and hepatic artery ligation or CCl4 administration. A comparative study with dopamine agonists and

- somatostatin. *Life Sci* 1993;53:PL291-PL296.
16. Reynaert H, Vaeyens F, Qin H, Hellemans K, Chatterjee N, Winand D, et al. Somatostatin suppresses endothelin-1-induced rat hepatic stellate cell contraction via somatostatin receptor subtype 1. *Gastroenterology* 2001;121:915-930.
  17. Fort J, Oberti F, Pilette C, Veal N, Gallois Y, Douay O, et al. Antifibrotic and hemodynamic effects of the early and chronic administration of octreotide in two models of liver fibrosis in rats. *Hepatology* 1998;28:1525-1531.
  18. Reynaert H, Rombouts K, Vandermonde A, Urbain D, Kumar U, Bioulac-Sage P, et al. Expression of somatostatin receptors in normal and cirrhotic human liver and in hepatocellular carcinoma. *Gut* 2004;53:1180-1189.
  19. Reynaert H, Rombouts K, Jia Y, Urbain D, Chatterjee N, Uyama N, et al. Somatostatin at nanomolar concentration reduces collagen I and III synthesis by, but not proliferation of activated rat hepatic stellate cells. *Br J Pharmacol* 2005;146:77-88.
  20. Borie R, Fabre A, Prost F, Marchal-Somme J, Lebtahi R, Marchand-Adam S, et al. Activation of somatostatin receptors attenuates pulmonary fibrosis. *Thorax* 2008;63:251-258.
  21. Duran-Prado M, Morell M, Delgado-Maroto V, Castaño JP, Aneiros-Fernandez J, De Lecea L, et al. Cortistatin inhibits migration and proliferation of human vascular smooth muscle cells and decreases neointimal formation on carotid artery ligation. *Circ Res* 2013;112:1444-1455.
  22. Morell M, Camprubí-Robles M, Culler MD, de Lecea L, Delgado M. Cortistatin attenuates inflammatory pain via spinal and peripheral actions. *Neurobiol Dis* 2014;63:141-154.
  23. Liu Y, Lin F, Fu Y, Chen W, Liu W, Chi J, et al. Cortistatin inhibits arterial calcification in rats via GSK3 $\beta$ / $\beta$ -catenin and protein kinase C signalling but not c-Jun N-terminal kinase signalling. *Acta Physiol (Oxf)* 2018;223:e13055.
  24. Wang M, Gong Q, Zhang J, Chen L, Zhang Z, Lu L, et al. Characterization of gene expression profiles in HBV-related liver fibrosis patients and identification of ITGBL1 as a key regulator of fibrogenesis. *Sci Rep* 2017;7:43446.
  25. Mas VR, Maluf DG, Archer KJ, Yanek K, Kong X, Kulik L, et al. Genes involved in viral carcinogenesis and tumor initiation in hepatitis C virus-induced hepatocellular carcinoma. *Mol Med* 2009;15:85-94.
  26. Moylan CA, Pang H, Dellinger A, Suzuki A, Garrett ME, Guy CD, et al. Hepatic gene expression profiles differentiate presymptomatic patients with mild versus severe nonalcoholic fatty liver disease. *Hepatology* 2014;59:471-482.
  27. Percie du Sert N, Hurst V, Ahluwalia A, Alam S, Avey MT, Baker *Met al* . The ARRIVE guidelines 2.0: Updated guidelines for reporting animal research. *Br J Pharmacol* 2020;177:3617-3624.
  28. Córdoba-Chacón J, Gahete MD, Pozo-Salas AI, Martínez-Fuentes AJ, De Lecea L, Gracia-Navarro F, et al. Cortistatin is not a somatostatin analogue but stimulates prolactin release and inhibits GH and ACTH in a gender-dependent fashion: potential role of ghrelin. *Endocrinology* 2011;152:4800-4812.
  29. Seki E, De Minicis S, Österreicher CH, Kluwe J, Osawa Y, Brenner DA, et al. TLR4 enhances TGF-beta signaling and hepatic fibrosis. *Nat Med* 2007;13:1324-1332.
  30. Reddy GK, Enwemeka CS. A simplified method for the analysis of hydroxyproline in biological tissues. *Clin Biochem* 1996;29:225-229.
  31. Weiskirchen S, Tag CG, Sauer-Lehnen S, Tacke F, Weiskirchen R. Isolation and culture of primary murine hepatic stellate cells. *Methods Mol Biol* 2017;1627:165-191.
  32. Gautier L, Cope L, Bolstad BM, Irizarry RA. “affy—analysis of Affymetrix GeneChip data at the probe level.” *Bioinformatics* 2004;20:307-315.
  33. Ishak KG. Chronic hepatitis: morphology and nomenclature. *Mod Pathol* 1994;7:690-713.
  34. Standish RA, Cholongitas E, Dhillon A, Burroughs AK, Dhillon AP. An appraisal of the histopathological assessment of liver fibrosis. *Gut* 2006;55:569-578.
  35. Andres-Leon E, Nunez-Torres R, Rojas AM. miARma-Seq: a comprehensive tool for miRNA, mRNA and circRNA analysis. *Sci Rep* 2016;6:25749.
  36. Nikolayeva O, Robinson MD. edgeR for differential RNA-seq and ChIP-seq analysis: an application to stem cell biology. *Methods Mol Biol* 2014;1150:45-79.

37. Robinson MD, Oshlack A. A scaling normalization method for differential expression analysis of RNA-seq data. *Genome Biol* 2010;11:R25
38. Reeb PD, Bramardi SJ, Steibel JP. Assessing dissimilarity measures for sample-based Hierarchical Clustering of RNA sequencing data using Plasmode Datasets. *PLoS One* 2015;10:e0132310.
39. Ritchie ME, Phipson B, Wu D, Hu Y, Law CW, Shi W, et al. Limma powers differential expression analyses for RNA-sequencing and microarray studies. *Nucleic Acids Res* 2015;43:e47.
40. Yu G, Wang L-G, Han Y, He QY. clusterProfiler: an R package for comparing biological themes among gene clusters. *OMICS* 2012;16:284.
41. Curtis MJ, Alexander S, Cirino G, Docherty JR, George CH, Gienbycz MA *et al*. Experimental design and analysis and their reporting II: updated and simplified guidance for authors and peer reviewers. *Br J Pharmacol* 2018;175:987-993.
42. Xu L, Huy AY, Albanis E, Arthur MJ, O’Byrne SM, Blaner WS, et al. Human hepatic stellate cell lines, LX-1 and LX-2: new tools for analysis of hepatic fibrosis. *Gut* 2005; 54:142-151.
43. Hernandez-Gea V, Friedman SL. Pathogenesis of liver fibrosis. *Annu Rev Pathol* 2011;6:425-456.
44. Hagashi T, Friedman SL, Hoshida Y. Hepatic stellate cells as key target in liver fibrosis. *Adv Drug Deliv Rev* 2017;121:27-42.
45. De Minicis S, Seki E, Uchinami H, Kluwe J, Zhang Y, Brenner DA, et al. Gene expression profiles during hepatic stellate cell activation in culture and in vivo. *Gastroenterology* 2007;132:1937-1946.
46. Tsuchida T, Friedman SL. Mechanisms of hepatic stellate cell activation. *Nat Rev Gastroenterol Hepatol* 2017;14:397-411.
47. Troeger JS, Mederacke I, Gwak G-Y, Dapito DH, Mu X, Hsu CC, et al. Deactivation of hepatic stellate cells during liver fibrosis resolution in mice. *Gastroenterology* 2012;143:1073-1083.
48. Kisseleva T, Cong M, Paik Y, Scholten D, Jiang C, Benner C, et al. Myofibroblasts revert to an inactive phenotype during regression of liver fibrosis. *Proc Natl Acad Sci USA* 2012;109:9448-9453.
49. Kisseleva T, Brenner D. Molecular and cellular mechanisms of liver fibrosis and its regression. *Nat Rev Gastroenterol Hepatol* 2021;18:151-166.
50. Ibañez-Costa A, Luque RM, Castaño JP. Cortistatin: a new link between the growth hormone/prolactin axis, stress and metabolism. *Growth Horm IGF Res* 2017;33:23-27.
51. Jordan VK, Zaveri HP, Scott DA. 1p36 deletion syndrome: An update. *Appl Clin Genet* 2015;8:189-200.
52. Giordano R, Picu A, Bonelli L, Broglio F, Prodám F, Grottoli S, et al. The activation of somatostatinergic receptors by either somatostatin-14 or cortistatin-17 often inhibits ACTH hypersecretion in patients with Cushing’s disease. *Eur J Endocrinol* 2007;157:393-398.
53. Rol A, Todorovski T, Martin-Malpartida P, Escola A, Gonzalez-Rey E, Aragon E, et al. Structure-based design of a cortistatin analogue with immunoregulatory activity in models of inflammatory bowel disease. *Nat Commun* 2021;12:1869.

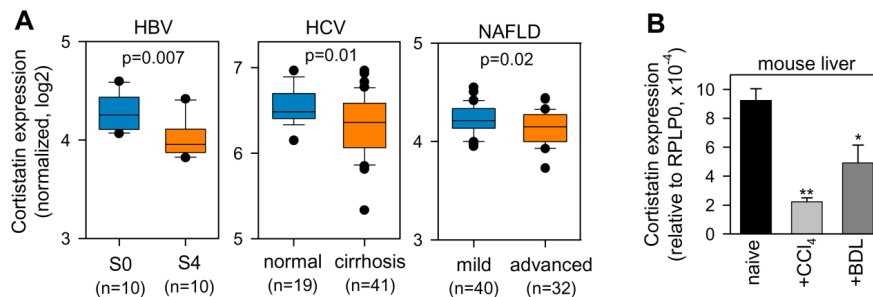


**Fig. 1. Cortistatin gene expression is downregulated in mouse and human fibrotic livers.** (A) The levels of cortistatin gene expression (normalized and expressed as log<sub>2</sub> values) were obtained from the Gene Expression Omnibus database based on the gene chips of fibrotic liver tissues associated to hepatitis B virus (HBV: healthy livers in Scheuer’s stage S0 versus high-fibrotic livers in Scheuer’s stage S4), hepatitis C virus-induced hepatocarcinoma (HCV: healthy versus cirrhotic livers), and nonalcoholic

fatty liver disease (NAFLD: livers in mild versus advanced stages). The number of patients in each group is shown. Data are shown with box plots and comparisons between groups were analyzed using unpaired two-tailed Student's t-test. (B) mRNA expression of cortistatin in livers collected from naïve mice, mice with CCl<sub>4</sub>-induced toxic fibrosis and mice subjected to bile duct ligation (BDL)-induced cholestatic fibrosis (5 mice/group). Gene expression was determined by real-time qPCR and data are relative to the expression of housekeeping RPLP0 gene. Data are the mean ± SEM. \*p < 0.05, \*\*p < 0.01 vs. naïve liver, using unpaired two-tailed Student's t-test.

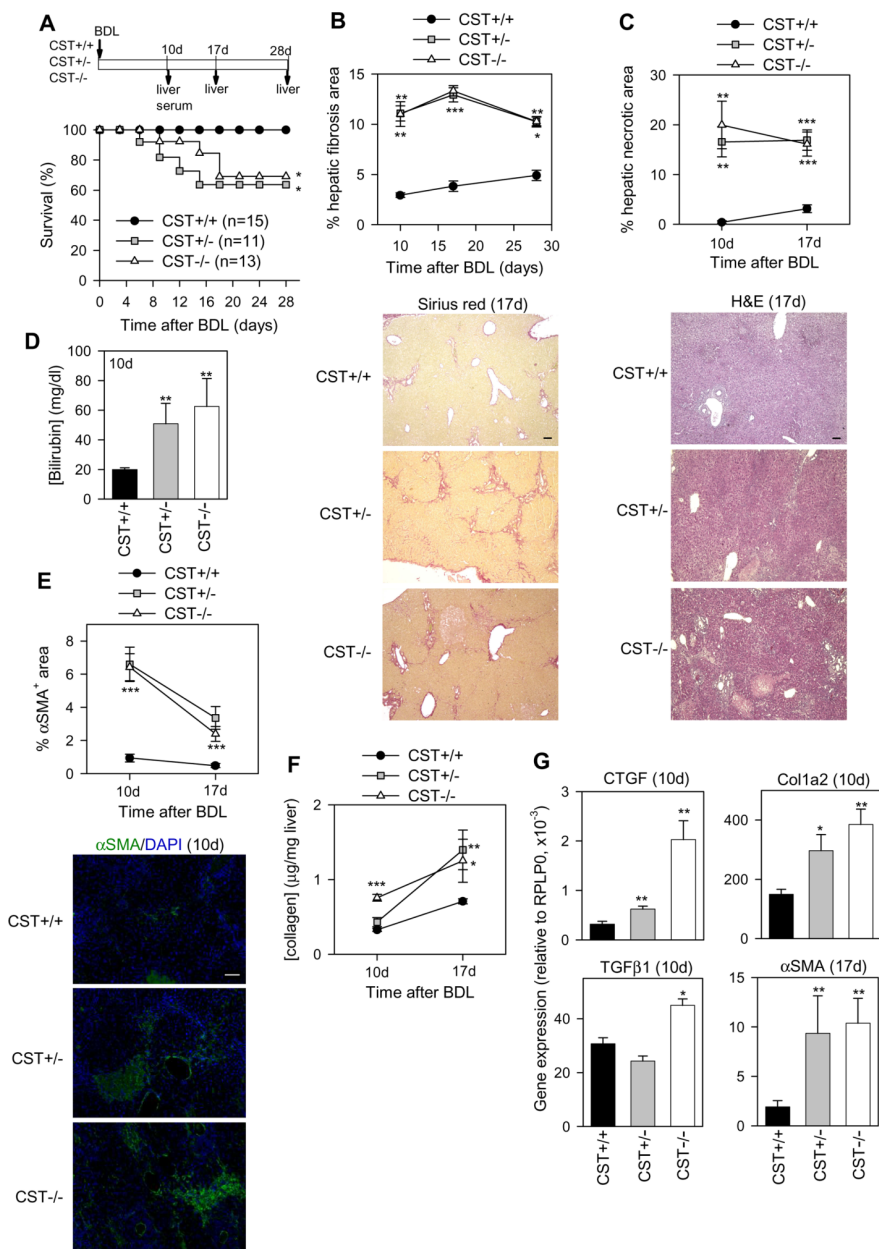


**Fig. 2. Deficiency in cortistatin exacerbates cholestatic-induced liver fibrosis.** Hepatic fibrosis was induced in wild-type (*CST*<sup>+/+</sup>), partially-deficient (*CST*<sup>+/-</sup>) or totally-deficient (*CST*<sup>-/-</sup>) mice for cortistatin by using a model of chronic cholestatic obstruction by bile duct ligation (BDL). (A) Survival

was monitored and liver and sera were collected as depicted in the diagram. **(B)** Extension of fibrosis was quantified in Sirius red-stained liver sections (5-15 mice/group, scale bars: 200- $\mu\text{m}$ ). **(C)** Histopathological damage and extension of necrosis area were determined in hematoxylin/eosin (H&E)-stained liver sections (5-13 mice/group; scale bars: 100- $\mu\text{m}$ ). Fig. S2A shows images at higher magnification. **(D)** Serum levels of direct bilirubin were measured 10 days after BDL (5 mice/group). **(E)** Presence of myofibroblasts was determined by measuring the area with  $\alpha$ -smooth muscle actin ( $\alpha\text{SMA}$ )-positive immunofluorescence in liver sections (5-7 mice/group, scale bars: 100- $\mu\text{m}$ ). **(F-G)** Markers of hepatic fibrosis were determined at the indicated times by measuring collagen contents in liver protein extracts and mRNA expression of connective-tissue growth factor (CTGF),  $\alpha\text{SMA}$ , collagen1- $\alpha 2$  (Col1a2) and TGF $\beta 1$  (5-8 mice/group). Data are the mean $\pm$ SEM. \* $p < 0.05$ , \*\* $p < 0.01$ , \*\*\* $p < 0.001$  vs. *CST*<sup>+/+</sup> mice. All panels were analyzed with unpaired two-tailed Student's t-test, unless survival that was analyzed with Kaplan-Meier log-rank test.

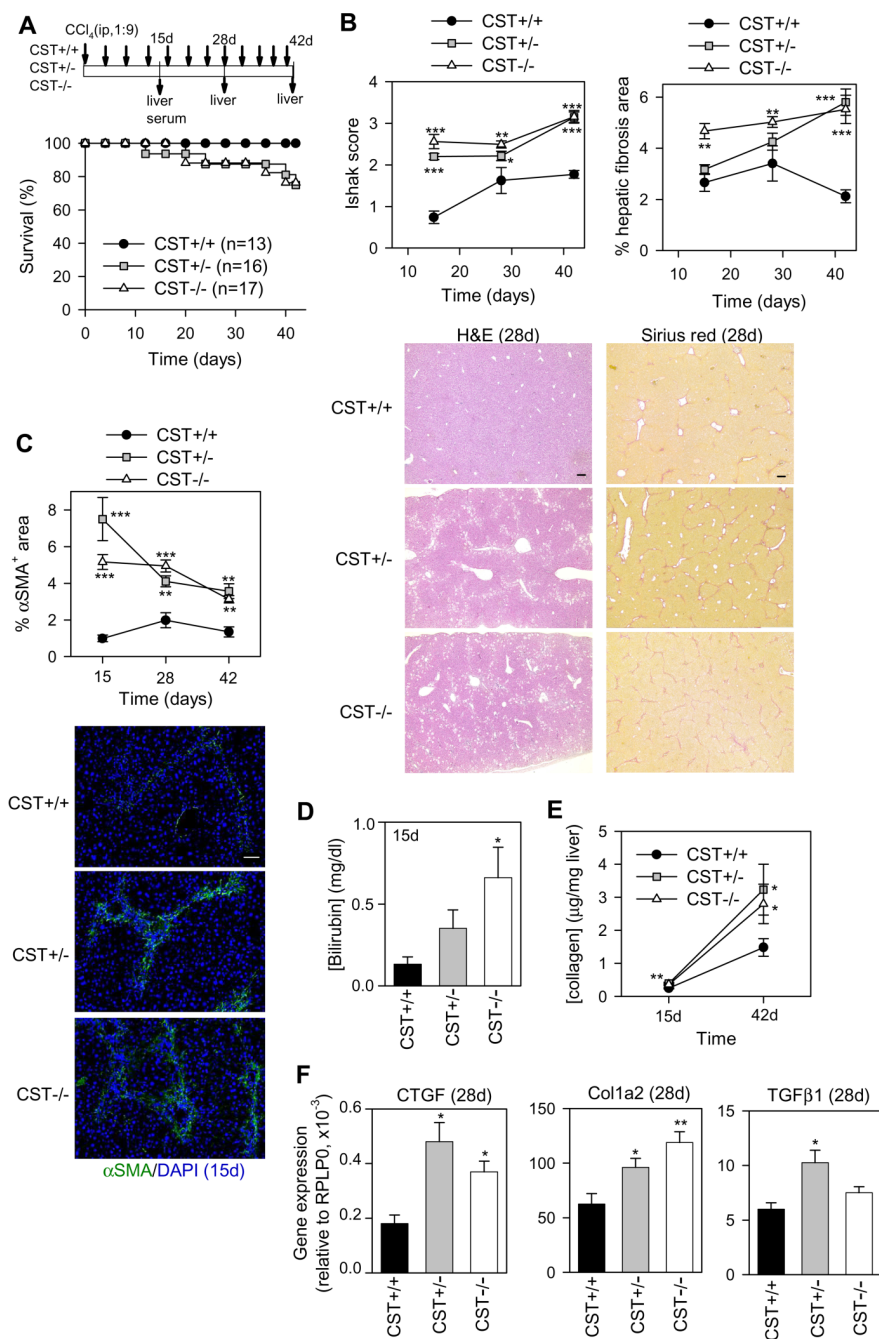


**Figure 3. Deficiency in cortistatin increases disease severity in an experimental model of toxic-induced liver fibrosis.** Chronic hepatic fibrosis was induced in wild-type ( $CST^{+/+}$ ), partially-deficient ( $CST^{+/-}$ ) or totally-deficient ( $CST^{-/-}$ ) mice for cortistatin by injecting repetitive low doses of the toxic agent  $CCl_4$  as depicted in the diagram. (A) Survival was daily monitored. (B) Fibrosis-induced hepatic damage was quantified by using histopathological Ishak score and the extension of fibrosis in hematoxylin/eosin (H&E)- and Sirius red-stained liver sections (5-15 mice/group; scale bars: 200- $\mu$ m). Fig. S2B displays images at higher magnification. (C) Presence of  $\alpha$ -smooth muscle actin ( $\alpha$ SMA)-positive myfibroblasts was determined by immunofluorescence analysis of liver sections (5-13 mice/group; scale bars: 100- $\mu$ m).

(D) Serum levels of direct bilirubin at day 15 (5 mice/group). (E-F) Markers of hepatic fibrosis were determined at the indicated times by measuring collagen contents in liver protein extracts (5-13 mice/group) and mRNA expression of connective-tissue growth factor (CTGF), collagen1- $\alpha 2$  (Col1a2) and TGF $\beta 1$  (5-11 mice/group). \* $p < 0.05$ , \*\* $p < 0.01$ , \*\*\* $p < 0.001$  vs. *CST*<sup>+/+</sup> mice. All panels were analyzed with unpaired two-tailed Student's t-test, unless survival that was analyzed with Kaplan-Meier log-rank test, and Ishak scores that were analyzed with Mann-Whitney U-test.

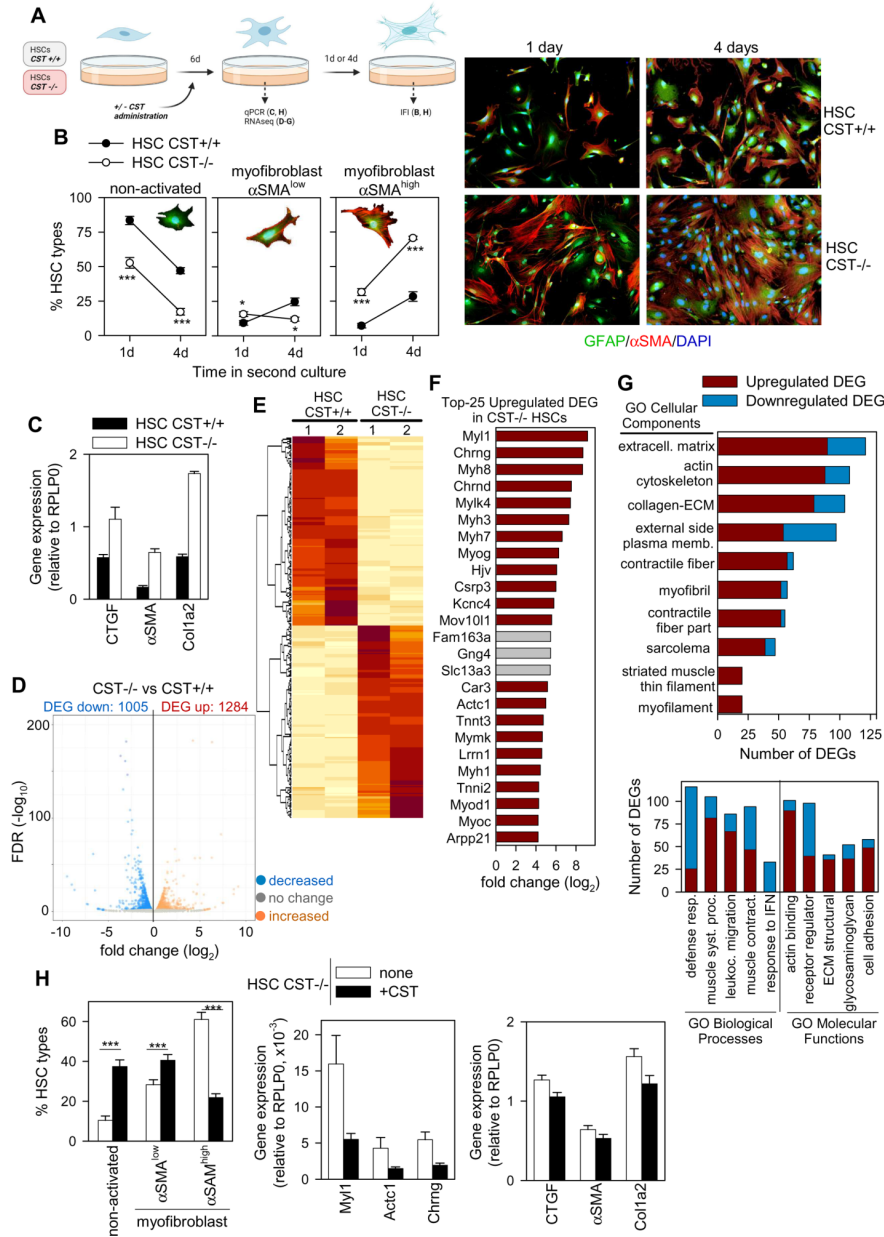


**Fig. 4. Cortistatin-deficient HSCs show exacerbated fibrotic responses and excessive differentiation capacity to activated myfibroblasts.** (A) Nonparenchymal HSC-enriched fractions were isolated from wild-type (*CST*<sup>+/+</sup>) and cortistatin-deficient (*CST*<sup>-/-</sup>) livers and cultured as described in the diagram. (B) Analysis of glial fibrillary acidic protein (GFAP) and  $\alpha$ -smooth muscle actin ( $\alpha$ SMA) expression by im-

munofluorescence of HSC cultures to determine the percentage of non-activated HSCs ( $GFAP^+/\alpha SMA^-$ ), myofibroblasts  $GFAP^+/\alpha SMA^{low}$  and activated myofibroblasts  $\alpha SMA^{high}$  (with stress fibers) at different times ( $n=18$  for 6d+1d cultures,  $n=5$  for 6d+4d cultures). Representative images for each cell type used to the analysis are shown as examples. (C) Expression of profibrogenic mediators in HSCs after primary cultures ( $n=3$  cultures by duplicates). (D-G) Gene expression profile in  $CST^{+/+}$  and  $CST^{-/-}$  HSCs analyzed by next-generation RNA sequencing. (D) Volcano plot depicting the differentially expressed genes (DEGs, with false discovery rate  $FDR-p<0.05$ ) between  $CST^{-/-}$  and  $CST^{+/+}$  HSCs (description for all DEGs is included in table S5). (E) Unsupervised hierarchical clustering of the 640-top DEGs (with  $\log_2$  fold-change  $>1$  or  $<-1$ ) separated the samples into two major groups. (F) Fold-change expression of the top-25 upregulated DEGs in  $CST^{-/-}$  HSCs. Red bars correspond to muscle-related genes (table S1 shows a detailed description of these DEGs). (G) Gene ontology (GO) analysis of the DEGs between  $CST^{-/-}$  and  $CST^{+/+}$  HSCs. The top-10 or top-5 terms are included. Red and blue bar-segments correspond to numbers of upregulated and downregulated DEGs, respectively. All DEGs in each GO term are listed in tables S2 to S4. (H) Effect of cortistatin addition every other day to primary cultures of  $CST^{-/-}$  HSCs on myofibroblast activation/differentiation (immunofluorescence at day 4,  $n=11$  cultures) and expression of critical genes for myofibroblast activation and muscle differentiation ( $n=3$  cultures by duplicates). Data are the mean  $\pm$  SEM (unless data in F that are the mean). \* $p<0.05$ , \*\* $p<0.01$ , \*\*\* $p<0.001$ , unpaired two-tailed Student's t-test.

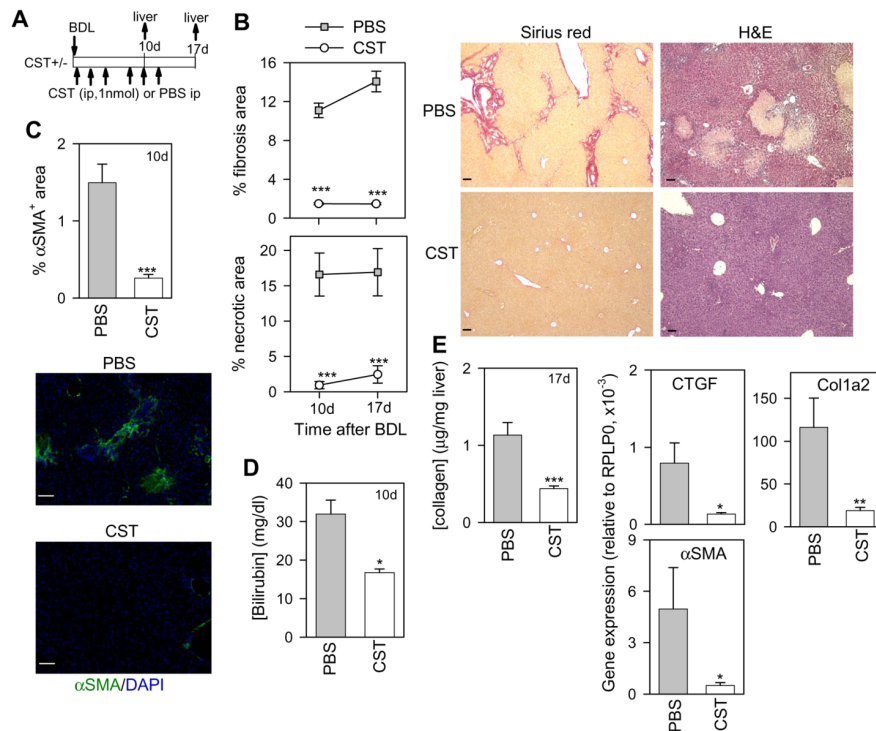


**Fig. 5. Administration of cortistatin reversed the exacerbated cholestasis-induced liver fibrosis observed in cortistatin-deficient mice.** (A) Hepatic fibrosis was induced by bile duct ligation (BDL) in partially-deficient ( $CST^{+/-}$ ) mice in cortistatin and treated i.p. with PBS or cortistatin as indicated in the diagram. (B) Extension of hepatic fibrosis and necrosis were determined in Sirius red- and H&E-stained sections (7-10 mice/group). (C) Presence of  $\alpha$ -smooth muscle actin ( $\alpha SMA$ )-positive myofibroblasts was quantified by immunofluorescence in liver sections (5-8 mice/group). (D) Serum levels of direct bilirubin were measured 10d post-BDL (5-8 mice/group). (E) Markers of hepatic fibrosis were determined by measuring collagen contents in liver protein extracts and gene expression of connective tissue growth factor (CTGF),  $\alpha SMA$  and collagen1- $\alpha 2$  (Col1a2) in liver mRNA isolated 17 days post-BDL (8-10 mice/group). Scale bars:

100- $\mu$ m. Data are the mean $\pm$ SEM. \* $p$ <0.05, \*\* $p$ <0.01, \*\*\* $p$ <0.001 vs. PBS-treated  $CST^{+/-}$  mice, unpaired two-tailed Student's t-test.

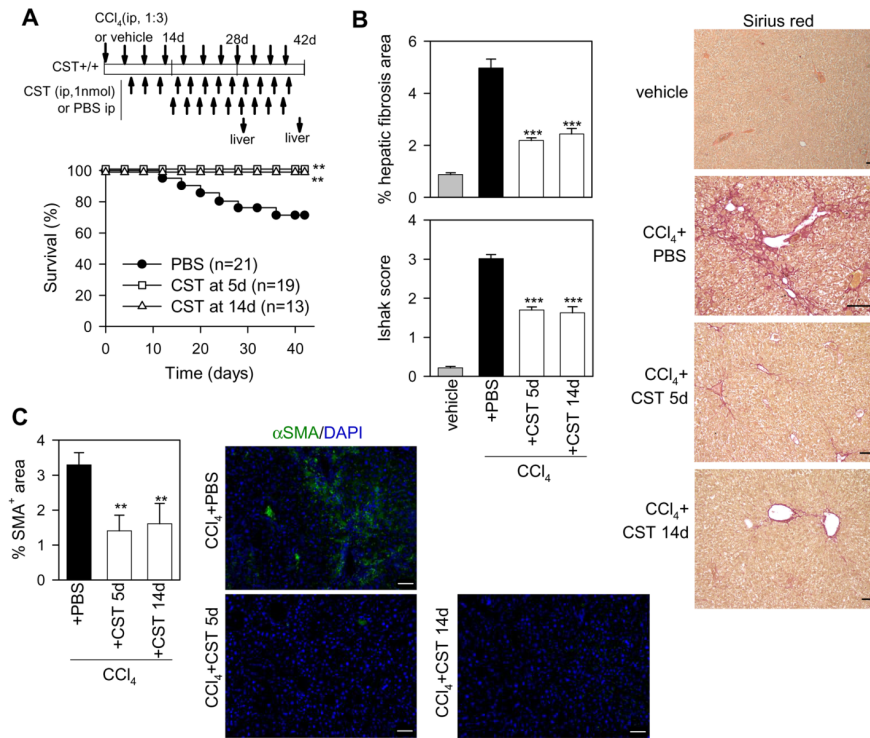


**Fig. 6. Treatment with cortistatin reduces mortality and disease severity in experimental toxic-induced hepatic fibrosis.** Severe hepatic fibrosis was induced in  $CST^{+/-}$  mice by repetitive injections of a high-dose of CCl<sub>4</sub>. Mice were then treated i.p. with PBS or with cortistatin starting on day 5 (early regime) or day 14 (delayed regime) as indicated in the diagram. Mice injected i.p. with vehicle (olive oil) instead CCl<sub>4</sub> were used as controls (n=5 mice). (A) Survival was daily monitored. (B) Hepatic fibrosis and damage were determined by using the histopathological Ishak score and quantifying fibrotic area in Sirius red-stained sections (13-20 mice/group). (C) The presence of  $\alpha$ -smooth muscle actin ( $\alpha$ SMA)-positive myofibroblasts in liver sections was determined by immunofluorescence (12 mice/group). Scale bars: 100- $\mu$ m. Data are the mean $\pm$ SEM. \*\* $p$ <0.01, \*\*\* $p$ <0.001 vs. PBS-treated mice. All panels were analyzed with unpaired two-tailed Student's t-test, unless survival that was analyzed with Kaplan-Meier log-rank test, and Ishak scores that were analyzed with Mann-Whitney U-test.